15th International Conference on Fluid Control, Measurements and Visualization
27-30 May, 2019, Naples, Italy

Natural convection induced by evaporation of heavier-than-air fluids

Nikolay A. Vinnichenko[1,*], **Alexey V. Pushtaev**[1], **Yulia Yu. Plaksina**[1], **Alexander V. Uvarov**[1]

[1]Faculty of Physics, Lomonosov Moscow State University, Moscow, Russia
[*]corresponding author: nickvinn@yandex.ru

Abstract Natural convection driven by evaporation of heavier-than-air fluids from the surface of the heated horizontal and vertical flat plates is studied both experimentally and numerically. The combined buoyancy effects of temperature and vapor density are shown to result in either downward or upward flow depending on the plate temperature and evaporating substance volatility and molar mass. For some substances (e.g., butanol) flow reversals are observed: solutal buoyancy is dominant for low and high temperatures of the heated plate leading to downward flow, whereas at moderate temperatures thermal buoyancy prevails resulting in upward convection. Refractive index fields are measured using Background Oriented Schlieren (BOS). Similarity between the temperature and vapor density fields associated with heat and mass transfer analogy is used to obtain temperature and vapor density fields from experimental data. The validity of this approach is analyzed. Good agreement between experimental temperature and vapor density distributions and numerical simulations is obtained for ethanol vapor, which has Lewis number about 1.8. For butanol vapor, which has Lewis number about 2.5, similarity is violated and temperature and vapor density contributions to refractive index cannot be separated. This is also true for validity of simplified modeling using total expansion coefficient. Similarity is also shown to be violated for hot liquid evaporation from a tank with conductive walls. In this case boundary conditions are dissimilar and upward convective flow of warm clean air near the outer surface of the tank walls is observed, which entrains the heavy vapor.
Keywords: natural convection, background oriented schlieren, evaporation, heat and mass transfer analogy

1 Introduction

Although most evaporation studies concern evaporation of water, many industrial applications (e.g., drying, combustion of liquid fuels, chemical processing, refrigeration, perfumery and pharmaceutics) involve evaporation of other fluids, which, unlike water vapor, are heavier-than-air. Natural convection flow of the air mixed with heavy vapor is driven by buoyancy effects of temperature and vapor density, which are aiding in case of evaporation from a cooled surface and opposing if the surface is heated. Convection due to combined buoyancy effects received less attention in comparison with purely thermal case, though similarity solutions of boundary-layer equations were obtained for semi-infinite vertical [1] and horizontal [2] isothermal flat plates. However, experimental studies are not numerous. This can be explained by the fact that both temperature and vapor density variations cause refractive index variations, measured with optical techniques widely used in gas dynamics. In order to separate temperature and vapor density contributions to refractive index one has either to perform simultaneous measurements using two different techniques or to employ supplementary assumption concerning the relation between temperature and vapor density distributions. Mach-Zehnder interferometer was used in [3] to study evaporation of benzene and n-heptane from the surface of porous vertical plate into the heated air flow. Temperature and vapor density distributions were assumed to be similar, which allowed separation of their contributions to refractive index. Interferometry was also used for vapor density measurements in vertical channel with CO_2 injection through a porous wall [4] and during evaporation of HFE-7000 pendant drop [5]. Traversing thermocouple was used to measure temperature in [4], whereas in [5] temperature variations were neglected. Vapor density measurements were performed using scanning Fourier transform infrared spectrometer [6].

It should be noted that heat and mass transfer analogy, from which similarity between the temperature and vapor density fields is derived, is strictly valid only for boundary-layer equations with Lewis number equal to unity (Reynolds analogy). It is often used for flows with non-unity Lewis number in the form of Chilton-Colburn analogy, but this is a useful empirical correlation rather than mathematical law, hence its validity can be limited. Obviously, if Prandtl and Schmidt numbers are different, thermal and concentration boundary layers have different thickness and temperature and vapor density distributions are dissimilar. Moreover, Reynolds analogy requires also similarity of boundary conditions and absence of source terms in heat and mass transfer equations. This can also be violated in real flows, e.g., due to presence of volume condensation. The validity

of using heat and mass transfer analogy for natural convection with combined buoyancy effects is even more problematic, since in this case heat and mass transfer affect each other.

Another important example of heavier-than-air vapor flow is naphthalene sublimation technique [7][8], which is still used for heat and mass transfer coefficients measurements despite the recent development of quantitative infrared thermography and heat flux sensors, since it avoids the conductive and radiative heat losses. Note that heat transfer coefficient measurements using naphthalene sublimation are also based on heat and mass transfer analogy. It was demonstrated that naphthalene sublimation results are not affected by humidity distribution in the flow [9], but thermal contribution to buoyancy can be comparable with the solutal one if the surface is heated or cooled.

This paper has two main objectives. The first is to study natural convection of heavier-than-air fluids both experimentally and numerically and to reveal the parameters, which determine the direction of convective flow. Our second objective is to examine the validity of using similarity of temperature and vapor density fields both for interpretation of experimental refractive index data and for simplified simulation using CFD code, which does not involve vapor transport. Experimental measurements are performed for ethanol and butanol evaporation from the surface of the heated horizontal and vertical flat plates using Background Oriented Schlieren (BOS) technique. Ethanol and butanol vapors are characterized by different values of Lewis number, which is key parameter for validity of temperature and vapor density fields similarity. Also, warm air saturated with butanol vapor can be either lighter or heavier in comparison with clean room-temperature air, which results in upward or downward convection for different plate temperatures, whereas ethanol evaporation, in absence of volume condensation, always leads to downward flow.

2 Problem formulation

Laminar convection of air–vapor mixture near the surface of a heated plate (horizontal or vertical) is described by 2D Navier-Stokes equations in low-Mach approximation:

$$\frac{\partial \rho}{\partial t} + \frac{\partial (\rho V_i)}{\partial X_i} = 0 \tag{1}$$

$$\rho \left(\frac{\partial V_i}{\partial t} + V_j \frac{\partial V_i}{\partial X_j} \right) = -\frac{\partial p}{\partial X_i} - \frac{2}{3} \frac{\partial}{\partial X_i} \left(\eta \frac{\partial V_j}{\partial X_j} \right) + \frac{\partial}{\partial X_j} \left[\eta \left(\frac{\partial V_i}{\partial X_j} + \frac{\partial V_j}{\partial X_i} \right) \right] + \rho g_i \tag{2}$$

$$\rho c_p \left(\frac{\partial T}{\partial t} + V_i \frac{\partial T}{\partial X_i} \right) = \frac{\partial}{\partial X_i} \left(\lambda \frac{\partial T}{\partial X_i} \right) + \left[-\frac{2}{3} \eta \frac{\partial V_k}{\partial X_k} \delta_{ij} + \eta \left(\frac{\partial V_i}{\partial X_j} + \frac{\partial V_j}{\partial X_i} \right) \right] \frac{\partial V_i}{\partial X_j} \tag{3}$$

$$\frac{\partial c}{\partial t} + V_i \frac{\partial c}{\partial X_i} = \frac{\partial}{\partial X_i} \left[\rho D \frac{\partial}{\partial X_i} \left(\frac{c}{\rho} \right) \right] \tag{4}$$

$$\rho = \frac{p_0 \mu_{air}}{RT} + \left(1 - \frac{\mu_{air}}{\mu_{vap}} \right) c \tag{5}$$

It is assumed that there is no condensation, Soret and Dufour effects are neglected. If vapor density and temperature variations are small, fluid properties, except density variation in Eq. (2), can be assumed constant, compressibility terms are neglected and Boussinesq approximation is obtained. Following boundary conditions for temperature, vapor density and velocity are to be imposed:

- at the plate surface: $T = T_{surf}$, $c = c_{sat}(T_{surf})$, $\vec{V} = 0$ (normal velocity due to evaporation is neglected).
- far from the plate: $T = T_0$, $c = c_0 = \varphi_0 c_{sat}(T_0)$, $\vec{V} = 0$.

T_0, φ_0 and c_0 are, respectively, temperature, relative vapor concentration and vapor density of the ambient air and T_{surf} is plate surface temperature.

If Lewis number $Le = \lambda / (\rho D c_p) = 1$, Eqs. (3) and (4) in Boussinesq approximation become identical and, since similar Dirichlet boundary conditions are imposed for temperature and vapor density both at the plate surface and far from the plate, T and c distributions must be similar:

$$\frac{T - T_0}{T_{surf} - T_0} = \frac{c - c_0}{c_{surf} - c_0} \tag{6}$$

Eq. (6) (or any other unique correspondence between T and c) enables one to obtain temperature and vapor density from refractive index field, measured with an optical technique, using Lorentz-Lorenz equation for air–vapor mixture at constant pressure (written here in CGS system of units, α is molecular polarizability volume)

$$\frac{n^2-1}{n^2+2} = \frac{4\pi N_A}{3}\left[\frac{\alpha_{air}}{\mu_{air}}\left(\frac{p_0\mu_{air}}{RT} - \frac{\mu_{air}}{\mu_{vap}}c(T)\right) + \frac{\alpha_{vap}}{\mu_{vap}}c(T)\right] \tag{7}$$

Moreover, if vapor density from Eq. (6) is substituted into Eq. (5) and linearization is performed with respect to temperature difference $(T-T_0)$, simplified equation of state is obtained, which contains only temperature variation:

$$\rho = \frac{p_0\mu_{air}}{RT_0}\left[1-\beta_{tot}\left(T-T_0\right)\right] + \left(1-\frac{\mu_{air}}{\mu_{vap}}\right)c_0, \tag{8}$$

where

$$\beta_{tot} = \frac{1}{T_0} - \left(1-\frac{\mu_{air}}{\mu_{vap}}\right)\frac{RT_0}{p_0\mu_{air}}\frac{c_{surf}-c_0}{T_{surf}-T_0} \tag{9}$$

is total expansion coefficient (TEC). This allows simplified modeling of the combined convection problem with CFD code, which does not support species transport simulation. Solutal contribution to buoyancy is taken into account by the second term in the right-hand side of Eq. (9) and vapor density, if required, can be easily found using Eq. (6).

Note, however, that if density variations are large or fluid properties dependence on temperature and vapor density is taken into account, Eqs. (3) and (4) are different, temperature and vapor density fields can be dissimilar and non-Boussinesq effects may arise. Thus, following conditions must be satisfied for similarity of temperature and vapor density distributions to be strictly valid:

- temperature and vapor density variations are small,
- Eqs. (3) and (4) do not contain extra terms (e.g., associated with volume condensation or thermal diffusion),
- boundary conditions for temperature and vapor density are similar,
- Lewis number $Le = 1$.

Volume condensation, if present, results in significant energy release and decrease of vapor density. Thus, it can modify the ratio between the thermal and solutal components of buoyancy. It occurs if the process path in c-T coordinates from $(T_{surf}, c_{sat}(T_{surf}))$ to $(T_0, \varphi_0 c_{sat}(T_0))$, followed by an air–vapor mixture parcel, crosses the saturated vapor curve. For water, ethanol and butanol evaporation into clean air volume condensation takes place only if temperature difference $(T_{surf}-T_0)$ exceeds 15 K. In the present study surface temperature values below or slightly above this limit are considered and the effect of volume condensation is neglected.

The convective flow direction can be estimated by comparison of the surface and ambient values of air–vapor mixture density. Using Eq. (5) and boundary conditions given above ($\varphi_0 = 0$),

$$\frac{\rho_{surf}}{\rho_0} = \left[1+\frac{p_{sat}(T_{surf})}{p_0}\left(\frac{\mu_{vap}}{\mu_{air}}-1\right)\right]\frac{T_0}{T_{surf}} \tag{10}$$

Thus, flow direction is determined by the temperature ratio, molar mass ratio and volatility of evaporating substance. Density ratio variation with surface temperature is shown in Fig. 1 for several heavier-than-air organic fluids. One can see that air saturated with ethanol or propanol vapor is always heavier than the ambient clean air, hence the convective flow is directed downwards. Butanol, decane and naphthalene have relatively small saturated vapor pressure, hence they exhibit flow reversals. At plate temperature slightly above the ambient temperature the solutal contribution is dominant and downward flow is expected. At moderately high temperatures of the plate vapor content becomes insufficient to support downward convection and thermal contribution to buoyancy results in upward flow. Finally, at high plate temperatures saturated vapor pressure

increases and the solutal contribution becomes dominant again leading to downward convection. Methanol, which has low boiling point, exhibits only the first flow reversal. Note that this is only simple argument based on mixture density values at the plate surface and far from the plate. As discussed in Section 5, flow direction is determined by the complete distribution of mixture density, which can be affected by Lewis number or by presence of volume condensation. The latter enhances thermal contribution to buoyancy and weakens the solutal one, thus promoting upward convection at high plate temperatures.

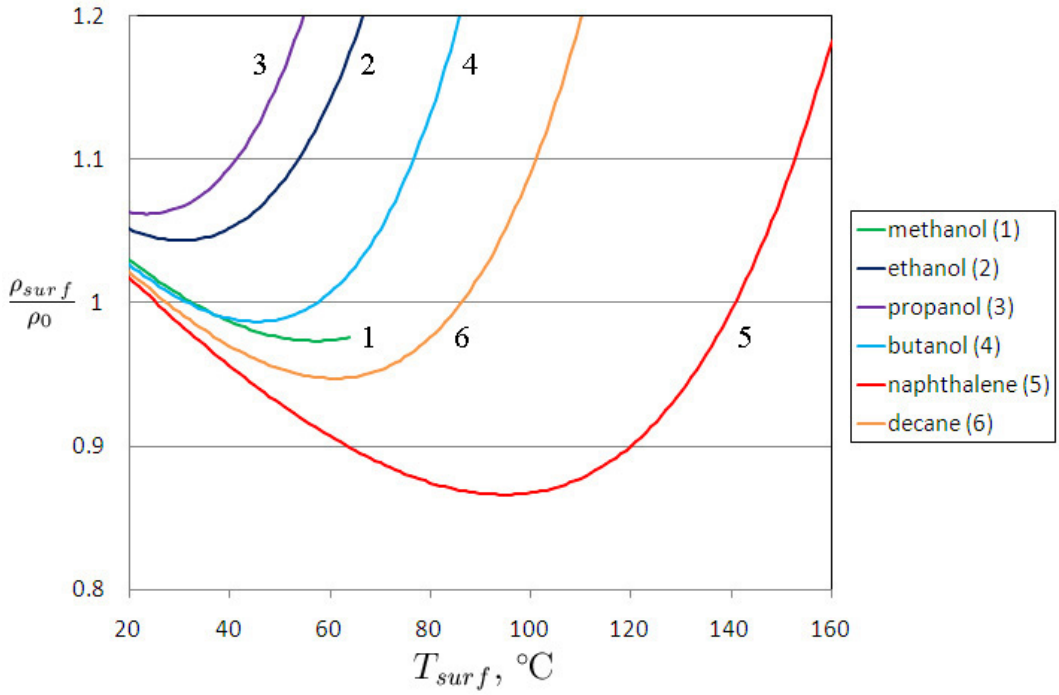

Fig. 1 Surface-to-ambient mixture density ratio for evaporation of selected organic compounds as function of plate surface temperature. $T_0 = 25°C$, $\varphi_0 = 0$.

3 Experimental technique and equipment

Flat heating element covered with smooth-faced cloth is mounted on textile laminate plate $28 \times 15 \times 0.7$ cm used as support. Before the measurements the cloth is wetted with liquid (ethanol or butanol) and heating is initiated. For evaporation from the surface of the vertical heated plate narrow heater 10.3×3.6 cm is used, whereas in experiments with horizontal heated plate wide heater 10.3×11.4 cm is employed, since lower values of refractive index gradient in the boundary layer require larger thickness of the schlieren object. The temperature of the cloth surface, measured with infrared pyrometer MLG 225 Laborant (wavelength band 8–14 μm, accuracy ± 1.5 K, surface emissivity value 0.95 is used), and the ambient air temperature, measured with thermocouple, determine the similarity line Eq. (6) and provide boundary conditions for numerical simulations. The ambient air temperature also determines the ambient air refractive index, which is used as far-from-the-plate boundary condition for Poisson equation in BOS data processing.

BOS [10] is quantitative visualization technique based on digital evaluation of the distortion of background pattern photographed through the flow under investigation. The distorted images are compared to the reference image, taken through the medium with constant refractive index, and the displacement field is determined, which is proportional to path-averaged refractive index gradient. Usually, background patterns resembling PIV images are used and the displacement field is found with cross-correlation interrogation algorithms. Then, the path-averaged 2D refractive index field can be obtained from its first spatial derivatives by solving Poisson equation. BOS was already used to measure air temperature fields above a heated horizontal plate [11] and to determine concentration in an isothermal hydrogen jet [12]. In the present study the refractive index depends both on temperature and vapor density, hence supplementary relation is required, which is provided by

assumption that temperature and vapor density distributions are similar. Numerical solution of Lorentz-Lorenz equation for air–vapor mixture Eq. (7) enables one to obtain temperature and vapor density fields. However, their accuracy (unlike the accuracy of refractive index field) is strongly dependent on the validity of similarity assumption. Following values of molecular polarizability volumes are used: air – $2.118 \cdot 10^{-29}/(4\pi)$ m^3, ethanol – $5.41 \cdot 10^{-30}$ m^3, butanol – $9.5 \cdot 10^{-30}$ m^3. Note that the accuracy of these values affects the accuracy of separation of temperature and vapor density contributions to refractive index in BOS experiment and the accuracy of refractive index calculation in numerical simulations.

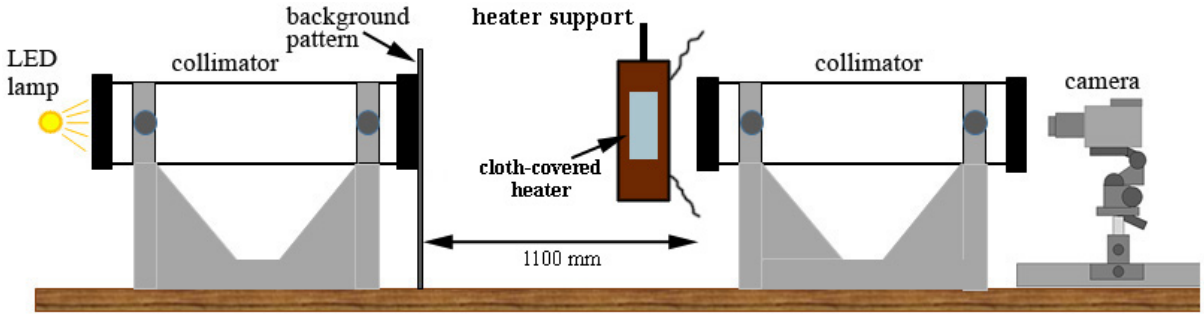

Fig. 2 Schematic of experimental setup with vertical heated plate.

Optical setup for BOS measurements is shown in Fig. 2. The background pattern, composed of transparent square dots randomly distributed over a black area, is printed on a transparent film using the equipment for offset printing. It is attached to a glass sheet and backlit with 14 W LED lamp. As in [13], two collimating tubes are used to make light beams nearly parallel to the optical axis, thus suppressing the perspective effect (telecentric BOS setup). Images are taken at 1 fps with Canon EOS 700D camera equipped with Canon EF 75–300 mm f/4-5.6 lens. The plate is installed so that its heated surface is located in the middle of the frame. The background-to-flow distance, which determines BOS sensitivity, is varied from 47 cm to 98 cm, keeping maximal displacement in the range 3–13 pix. Typically, larger displacements are observed for ethanol evaporation, because ethanol is more volatile than butanol, which results in larger contribution of vapor density to refractive index at the same temperature. Image processing is performed using multi-pass direct cross-correlation interrogation with discrete window offset. In most cases two or three interrogation passes are performed, beginning with interrogation windows 32×32 with further refinement to 16×16 or 8×8. The final pass is performed with interrogation windows overlap 50%. Number of distorted images, taken to measure time-averaged refractive index fields, presents a trade-off between obtaining sufficient statistic and possible change of cloth surface temperature or vapor concentration due to evaporation. For nearly steady convection near the surface of the vertical heated plate 70 distorted images are taken. For unsteady evaporation from the surface of horizontal heated plate time-averaged fields are obtained using 150 distorted images. BOS measurement relative accuracy can be roughly estimated as the ratio of displacement noise (typically 0.2–0.3 pix) to maximal displacement. In the present study it varies from 2.3% to 10% for ethanol and butanol evaporation from the surface of vertical plates at 31.8°C and 23.9°C, respectively. More detailed discussion of different sources of error in BOS can be found in [14]. The most important one is displacement gradient, which can lead to cross-correlation interrogation failure, if it is large. In the present study it does not exceed 0.3 pix/pix, which is below the limit of multi-pass cross-correlation algorithm being used (0.4–0.5 pix/pix).

4 Numerical modeling

Equations (2), (3) and (4) are integrated using second-order semi-implicit scheme with third-order Runge-Kutta method for convective terms and Crank-Nicolson method for diffusion terms. Fractional-step method is used to find velocity and pressure corrections in order to satisfy the continuity equation Eq. (1). Spatial discretization involves central differences for diffusion terms and 4-points upwind differences for convective ones. Simulations are performed on a staggered grid refined near the plate surface. The same code, but without species transport, was used in [11] for simulation of natural convection of air above a horizontal heated plate.

Grid convergence study involved simulations using three different meshes with near-surface grid step 50, 100 and 200 μm. The obtained temperature, vapor density and velocity fields exhibit maximal discrepancy with respect to the finest mesh less than 1% for all grids. 180×200 and 120×210 grids with minimal step 200 μm are chosen for simulations of convection near the surface of the heated horizontal and vertical plates, respectively. The outer boundaries of the computational domain are located about 600 plate lengths from the plate. Simulations are further verified by comparison of the results for ethanol evaporation from the surface of the vertical plate at temperature 31.8°C with similarity solution [1]. Note that similarity solution was obtained using the equation of state linearized with respect to temperature and vapor density differences and for the fixed values of Prandtl and Schmidt numbers. Comparison of the horizontal temperature and vapor density profiles in the middle of the plate is shown in Fig. 3e and f for simulations with fixed *Pr* and *Sc*, simulations taking into account mixture properties variation with temperature and mass fraction and simplified modeling using total expansion coefficient. The effect of variable properties is less than 3% change of local temperature and vapor density values. Maximal value of convective flow velocity is slightly underestimated (by 4.5%) in simulations with fixed *Pr* and *Sc* in comparison with similarity solution. Simplified TEC model overestimates maximal velocity by 14%.

5 Results and discussion

5.1 Evaporation from a heated vertical plate

Fig. 3 presents the comparison of BOS measurements, numerical simulations using three different models (complete model either taking into account fluid properties variation or assuming fixed values of *Pr* and *Sc* and simplified TEC model Eq. (8) without species transport simulation) and similarity solution [1] for ethanol evaporation from the surface of the vertical plate with temperature 31.8°C. $X = 0$ corresponds to plate surface. Total Rayleigh number, based on mixture density difference $(\rho_0 - \rho_{surf})$ and plate length, is about $-2.1 \cdot 10^6$ and the convective flow is directed downwards. Good agreement is observed not only for refractive index data, but also for temperature and vapor density distributions, which indicates the validity of using similarity assumption for BOS data interpretation. Simplified TEC model, which also relies on similarity assumption, yields results, which are close to complete model and similarity solution [1]. Horizontal profiles of refractive index, temperature and vapor density for ethanol evaporation from the plate with temperature 17.4°C are shown in Fig. 4. The plate is not heated, its temperature is lower than the ambient, since the cloth is cooled by evaporating ethanol. Downward convection is observed, since thermal and solutal buoyancy effects are aiding in this case. Rayleigh number is again about $-2.1 \cdot 10^6$. The predictions of all numerical models are in good agreement with experimental results, which supports the validity of using similarity assumption for ethanol evaporation.

The results obtained for butanol evaporation at different plate temperatures (23.9°C and 46.1°C) are displayed in Fig. 5. Total Rayleigh numbers are, respectively, $-5.5 \cdot 10^5$ and $4 \cdot 10^5$. BOS data confirm that at 46.1°C the convective flow is directed upwards, as predicted by Fig. 1, whereas at 23.9°C downward flow is observed. Although experimental distributions of refractive index are in good agreement with results of numerical simulations (except TEC model), temperature profiles markedly differ, indicating violation of temperature and vapor density similarity assumption. This is due to relatively large Lewis number of air–butanol mixture (about 2.5 far from the plate surface – to be compared to about 1.8 for air–ethanol mixture). For butanol evaporation thermal boundary layer is significantly more thick than concentration one, which results in formation of the outer sublayer containing warm air with low vapor content. This leads to refractive index horizontal profile having a minimum in Fig. 5d. Similar minimum is also observed in simulated mixture density profiles (Fig. 6), since high temperature and low concentration of heavy vapor both result in low mixture density. If the plate is heated, the air in outer sublayer is lighter than the ambient air. This means that upward convection must be observed in the outer sublayer. However, air near the plate surface saturated with heavy vapor can be either lighter or heavier than the ambient air. If it is lighter, upward flow develops in the entire boundary layer. If it is heavier (see the curves for $T_{surf} = 28$°C or 70°C in Fig. 6), the flow becomes unsteady. For $T_{surf} = 28$°C upward convection in the outer sublayer coexists with downward flow near the plate surface and unsteady vortical perturbations are produced by Kelvin-Helmholtz instability. For $T_{surf} = 70$°C global upward flow driven by

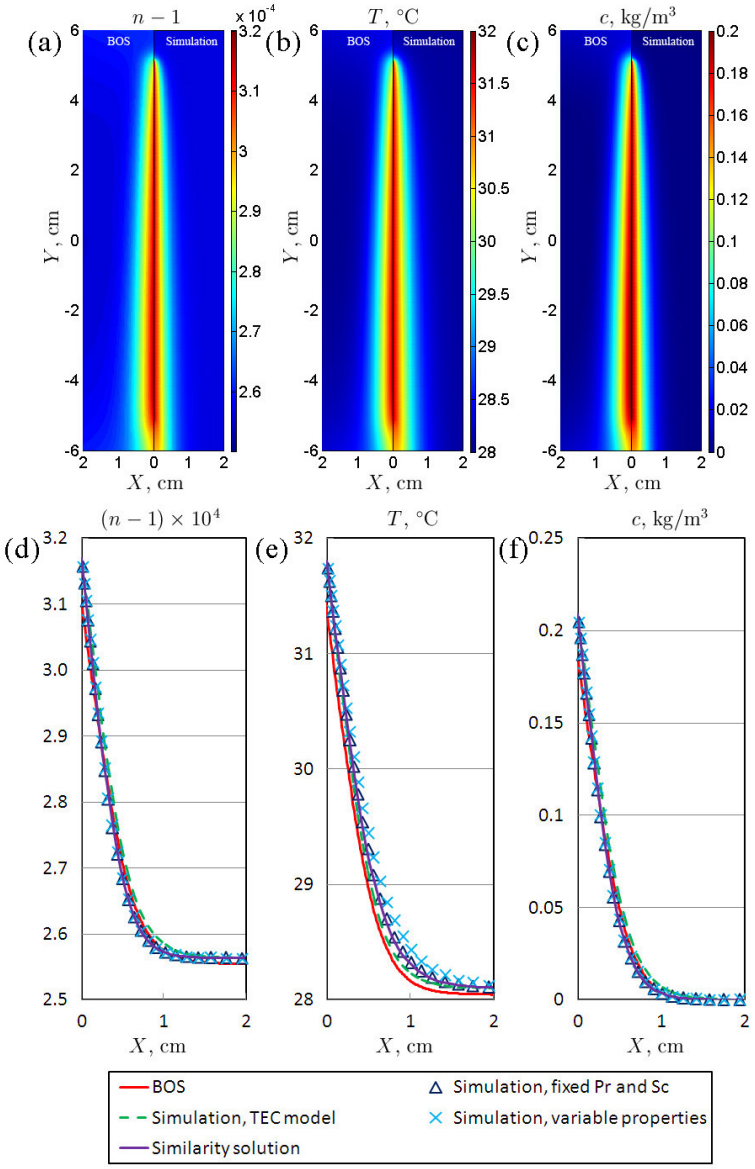

Fig. 3 Time-averaged fields of (a) refractive index, (b) temperature (°C) and (c) vapor density (kg/m^3) for ethanol evaporation from the surface of vertical heated plate. $T_{surf} = 31.8$°C, $T_0 = 28.1$°C. Left half of each panel represents BOS experimental data, right half shows the result of numerical simulation with fixed *Pr* and *Sc*. Horizontal profiles of (d) refractive index, (e) temperature and (f) vapor density in the middle of the plate ($Y = 0$).

light air of the outer sublayer is intermittently broken by the bursts of near-wall heavy air flowing downwards. Obviously, this is not described neither by the simple argument, based on mixture density ratio ρ_{surf}/ρ_0, nor by TEC model, which can also fail to predict the correct direction of convective flow for a fluid with large *Le*. It should be noted that at high temperatures of the plate volume condensation is to be taken into account. Volume condensation results in local temperature increase and vapor density decrease, thus affecting the mixture density distribution and promoting upward convection. BOS yields highly unsteady refractive index fields with apparent flow directed both upwards and downwards for plate temperatures above 60°C.

5.2 Evaporation from a heated horizontal plate

Comparison of BOS data and numerical simulations for ethanol evaporation from the surface of horizontal heated plate with temperature 30.5°C is shown in Fig. 7. Total Rayleigh number, based on the plate area-to-perimeter ratio, is $-2.6 \cdot 10^4$, which implies downward convection, hence the wet cloth-covered surface of

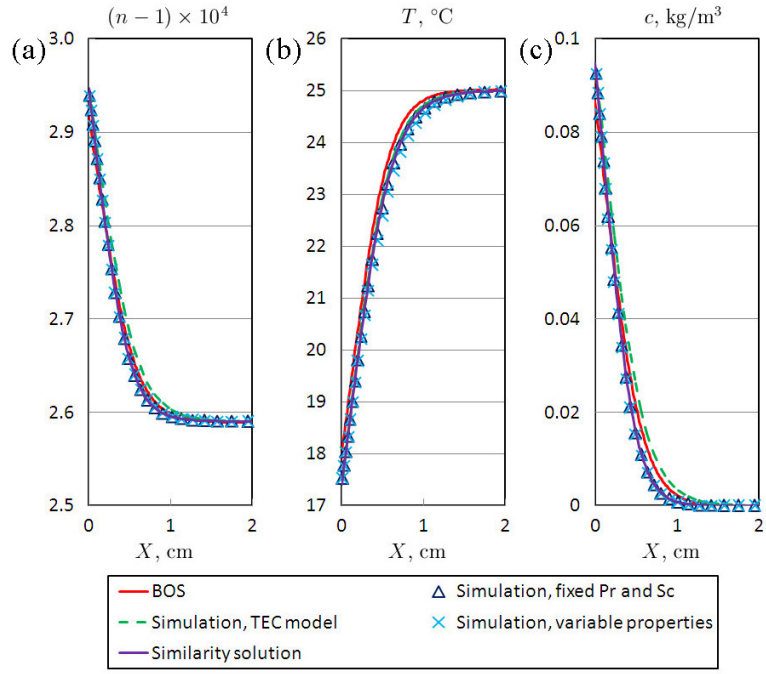

Fig. 4 Time-averaged horizontal profiles of (a) refractive index, (b) temperature and (c) vapor density at $Y = 0$ for ethanol evaporation from the surface of vertical plate. $T_{surf} = 17.4°C$, $T_0 = 25°C$.

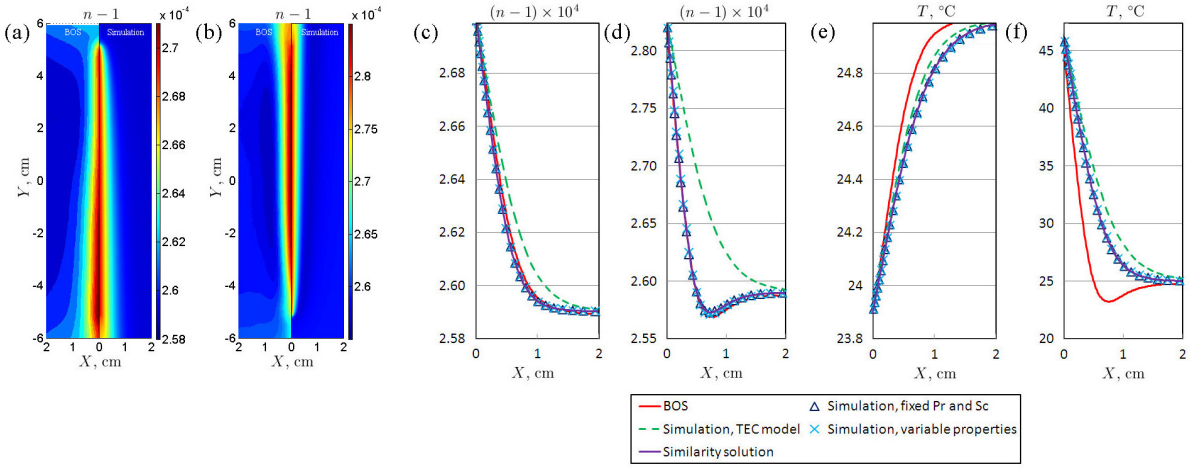

Fig. 5 Time-averaged fields of refractive index for butanol evaporation from the surface of vertical plate for (a) $T_{surf} = 23.9°C$, (b) $T_{surf} = 46.1°C$. $T_0 = 25°C$. Left half of each panel represents BOS experimental data, right half shows the result of numerical simulation with fixed *Pr* and *Sc*. Corresponding horizontal profiles of (c, d) refractive index and (e, f) temperature in the middle of the plate ($Y = 0$).

the plate is downward-facing. BOS is unable to resolve the uppermost 1.2-mm layer, probably due to larger thickness of schlieren object in comparison with the vertical plate case (11.4 cm and 3.6 cm, respectively) and associated perspective effect. Good agreement is observed in the outer part of the boundary layer, except that the central plume is more pronounced in simulations. Unlike the vertical plate case, the flow is unsteady, plumes are formed randomly at different locations along the plate both in experiment and simulations. In 2D simulations they are more localized in the central part of the plate, which results in existence of central plume in time-averaged field, whereas in path-averaged BOS data plumes are uniformly distributed along the plate surface. As for the vertical plate, experimental profiles of temperature and vapor density obtained using similarity assumption are close to the simulation data and simplified TEC model yields reasonable results.

The results, obtained for butanol evaporation from the surface of horizontal heated plate and presented

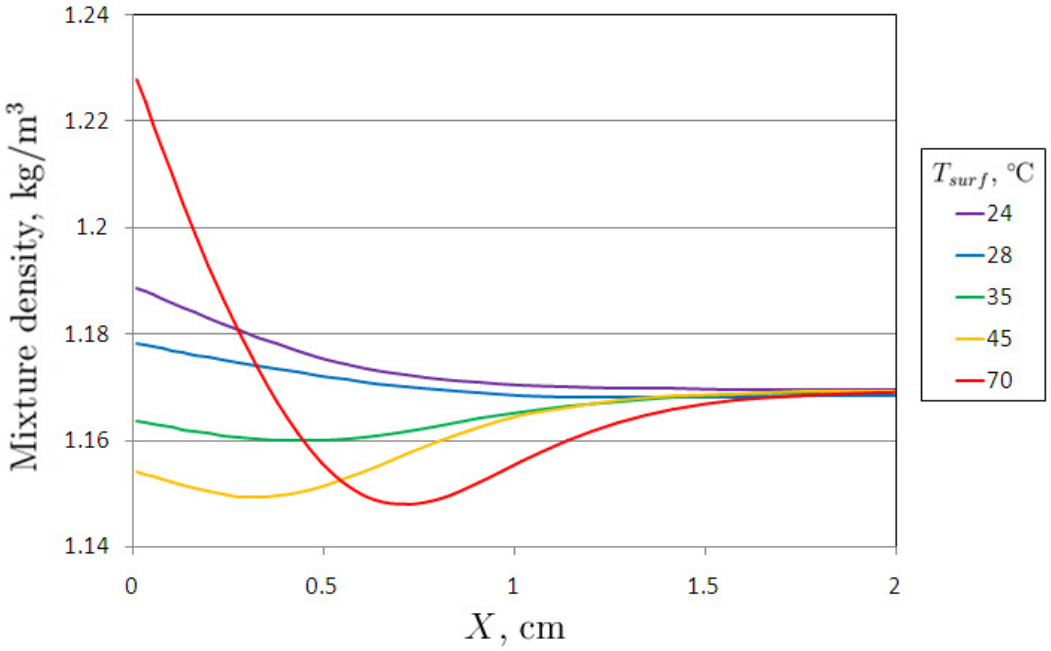

Fig. 6 Simulated mixture density horizontal profiles at $Y = 0$ for butanol evaporation from the surface of vertical plate for different values of plate temperature. $T_0 = 25°C$.

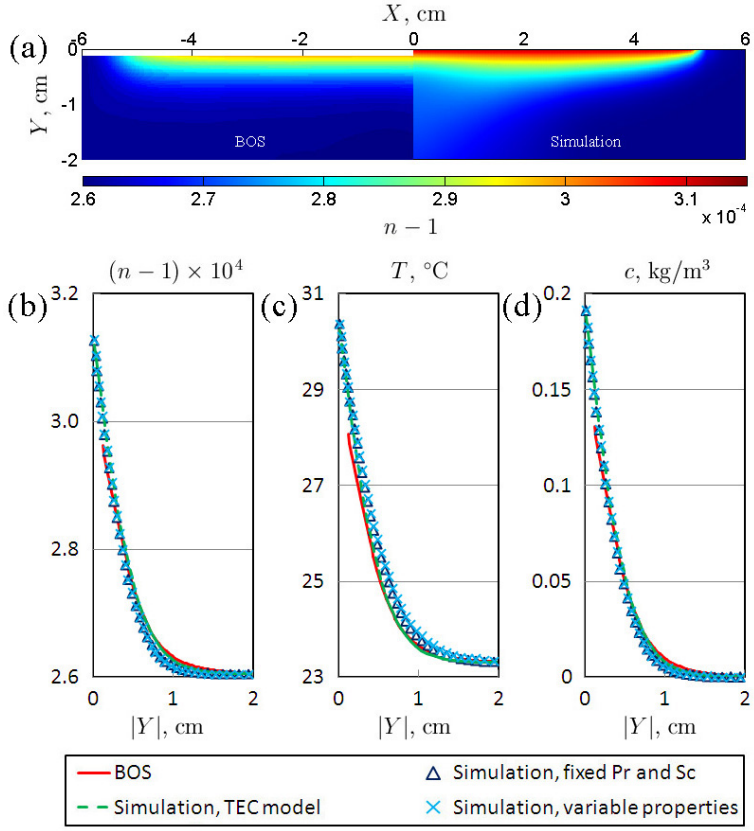

Fig. 7 (a) Time-averaged field of refractive index for ethanol evaporation from the lower surface of horizontal heated plate for $T_{surf} = 30.5°C$, $T_0 = 23.3°C$. Left half of the panel represents BOS experimental data, right half shows the result of numerical simulation with fixed *Pr* and *Sc*. Corresponding vertical profiles of (b) refractive index, (c) temperature and (d) vapor density at $|X| = 4$ cm.

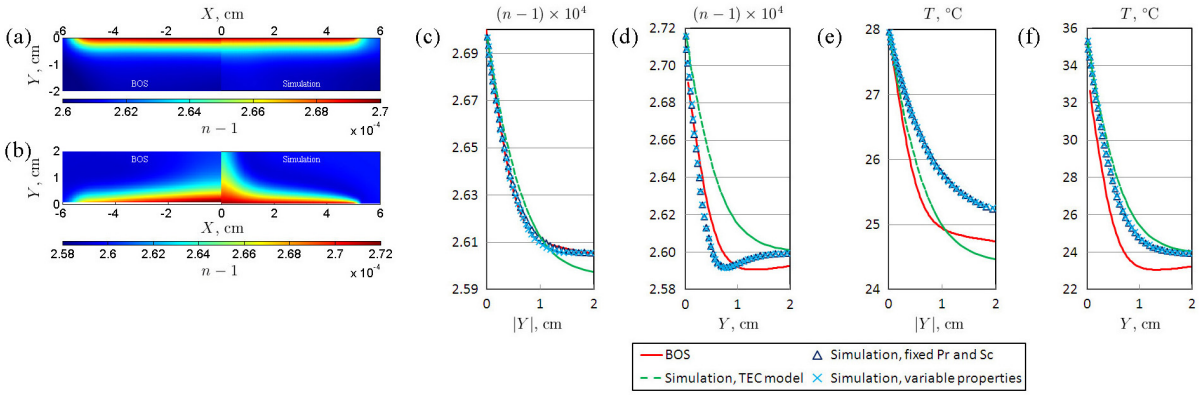

Fig. 8 Time-averaged fields of refractive index for butanol evaporation from the surface of horizontal heated plate for (a) $T_{surf} = 28°C$, $T_0 = 24.4°C$, (b) $T_{surf} = 35.5°C$, $T_0 = 23.9°C$. Left half of each panel represents BOS experimental data, right half shows the result of numerical simulation with fixed Pr and Sc. Corresponding vertical profiles of (c, d) refractive index and (e, f) temperature at $|X| = 4$ cm.

in Fig. 8, demonstrate downward convection at $T_{surf} = 28°C$ ($Ra = -3.2 \cdot 10^3$) and upward convection at $T_{surf} = 35.5°C$ ($Ra = 5.4 \cdot 10^3$). There is excellent agreement between experimental and numerical results for 28°C (Fig. 8a), whereas for 35.5°C (Fig. 8b) simulations predict the existence of well-pronounced central plume performing weak swaying and BOS exhibits main plume moving further away from the flow centerline and even several plumes in some frames. This leads to discrepancy in time-averaged distributions observed near the centerline. The origin of this discrepancy can be either 3D flow instability, which is not described by 2D simulations, or uncontrolled variation of temperature and vapor density along the plate surface in the experiment. Again, as in Fig. 5, temperature profiles, obtained from BOS using similarity assumption, and TEC model results are quite different from simulations using complete model – though the refractive index profiles in Fig. 8c agree well. This supports the conclusion that using similarity between temperature and vapor density fields leads to erroneous results for fluids with large Lewis number.

5.3 Evaporation of hot ethanol from a tank with conductive walls

For similarity of temperature and vapor density distributions to be valid it is required that similar boundary conditions are imposed for these quantities. This condition is satisfied for the substance evaporating from the surface of a solid plate. However, it can be violated for hot liquid evaporating from a container, if the container walls conduct heat. In fact, besides the boundary conditions representing air near the liquid surface and far from the tank, one more boundary is to be described – the outer surface of container walls. The walls conduct heat, but are impermeable to vapor. Thus, boundary conditions for temperature and vapor density are dissimilar. Fig. 9a, b presents time-averaged refractive index and temperature fields obtained using BOS for hot ethanol evaporation from an open rectangular tank $14.1 \times 7.2 \times 8.1$ cm made of 4-mm glass. The tank is installed so that its longest side is aligned with the camera line of sight. $Y = 0$ corresponds to top edge of the tank walls and ethanol surface is located at $Y = -2.5$ cm. Total Rayleigh number for air-side convection is $-3 \cdot 10^4$, air near the liquid surface is heavier than the ambient air, hence evaporation, driven by diffusion rather than convection, is expected. However, heat transfer through the tank walls leads to formation of upward flows of warm air free of vapor near the outer surface of tank walls. These flows are clearly seen in Fig. 9a as low refractive index regions near $X = \pm 4$ cm. Note that $n(T,c)$ for air–ethanol vapor mixture decreases with T and increases with c, hence regions with refractive index below the ambient value correspond to warm air with low vapor content. Convective flows of warm clean air deflect towards the tank center and entrain heavy air from the liquid surface, which results in upward convection-driven evaporation. Similarity of boundary conditions is violated, therefore temperature field obtained using similarity assumption is erroneous: warm air near the tank walls appears as cold air in Fig. 9b. This is explained by the fact that it has low refractive index and, if similarity assumption is used and vapor density contribution to refractive index is dominant in Eq. (7), $n(T, c(T))$ is monotonically increasing function of temperature. Fig. 9c, d, e presents the results of 2D numerical simulation with imposed

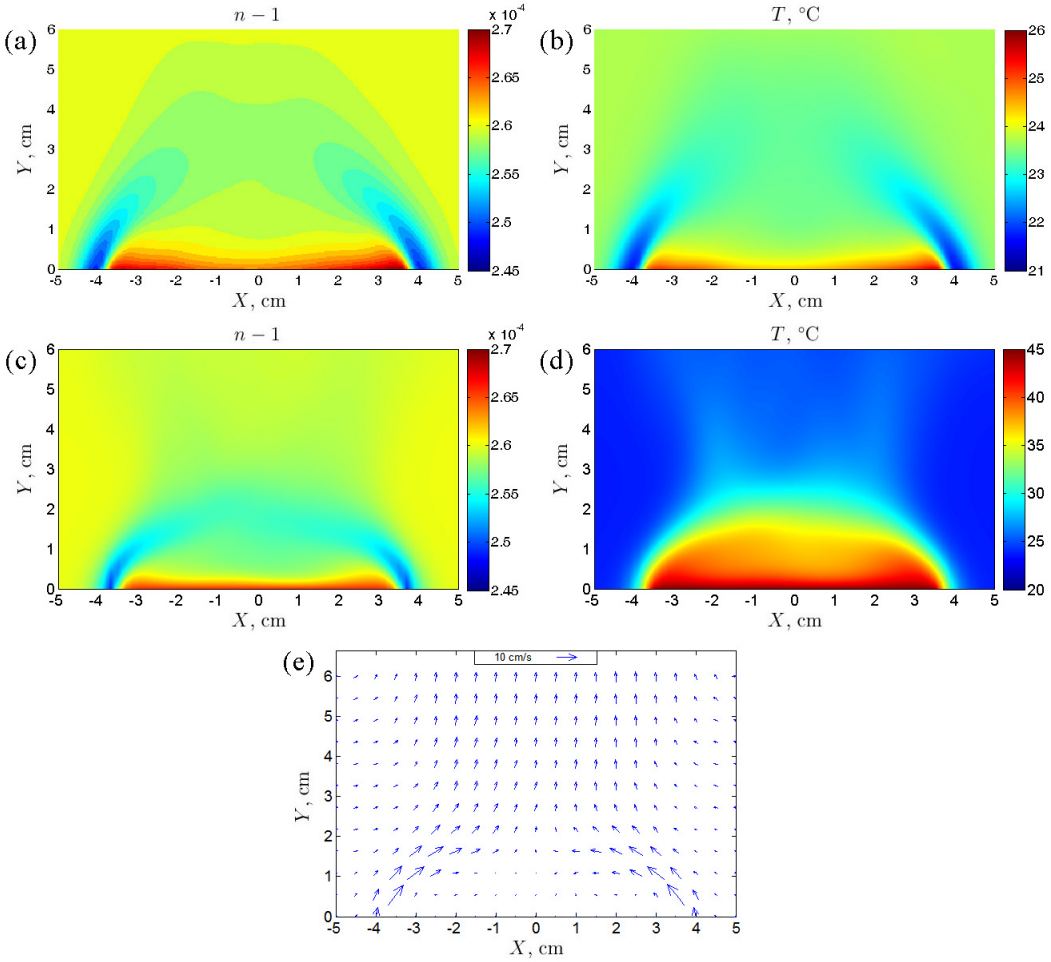

Fig. 9 Time-averaged fields of (a) refractive index and (b) temperature (°C) for ethanol evaporation from the glass tank obtained using BOS. Time-averaged fields of (c) refractive index, (d) temperature (°C) and (e) velocity obtained using 2D numerical simulation. $T_{surf} \approx 50$°C, $T_0 = 23.7$°C.

temperature of the tank walls outer surface 45°C. The refractive index fields are similar, but the temperature fields are totally different, indicating violation of similarity assumption. The velocity vector field (Fig. 9e) confirms upward convection. More accurate simulation should take into account heat conduction through the tank walls and air flows along the front and rear (with respect to BOS camera line of sight) walls, i.e. 3D structure of the flow. However, modeling of 3D conjugate heat transfer problem is beyond the scope of the present study.

6 Conclusions

In this study, refractive index fields during evaporation-driven natural convection of air–ethanol and air–butanol mixtures have been measured using BOS. Three flow configurations have been considered: evaporation from the surface of heated vertical plate, evaporation from the surface of heated horizontal plate and evaporation of hot liquid from a tank with conductive walls. Temperature and vapor density fields have been obtained from BOS data using similarity assumption associated with heat and mass transfer analogy and have been compared to numerical simulations, as well as the original refractive index fields.

It is demonstrated that convective flow direction depends on the plate surface and ambient temperatures, molar mass ratio of the considered air–vapor mixture and volatility of evaporating substance. Air–butanol mixture exhibits flow reversals depending on the plate temperature. If volume condensation is absent, air near the heated plate surface saturated with vapor is first heavier than the ambient clean air. Then, as plate temperature is increased, it becomes lighter and, again, heavier than the ambient air. Correspondingly, the convective flow

direction first switches from downward to upward, then it is expected to switch back to downward. However, since butanol vapor has Lewis number about 2.5, thermal boundary layer is significantly more thick than concentration one for evaporation from the surface of heated vertical plate. This results in existence of the outer sublayer, containing warm air with low vapor content, which is lighter than the ambient air and flows upwards. Also, at high plate temperatures volume condensation takes place, promoting upward convection. Thus, air–butanol mixture at high temperatures flows mostly upwards except of near-wall intermittent bursts of heavy air flowing downwards. In contrast, ethanol evaporation from a solid plate results in downward convection as long as volume condensation is absent, since Lewis number of ethanol vapor is only about 1.8.

The value of Lewis number is shown to be crucial for validity of using similarity assumption to derive temperature and vapor density from BOS data and for validity of simplified modeling using total expansion coefficient (TEC). For ethanol evaporation the obtained temperature and vapor density distributions are in good agreement with the results of numerical simulations and TEC model yields reasonable results. For butanol experimental and simulated refractive index fields agree well, but there is large discrepancy between the temperature and vapor density distributions obtained with BOS and simulations. TEC model, which also relies on similarity between temperature and vapor density distributions, yields erroneous results for butanol evaporation. This demonstrates that similarity assumption becomes invalid for fluids with Lewis number larger than 2. Also, similarity can be violated if one more boundary is present with dissimilar conditions for temperature and vapor density. This is illustrated with evaporation of hot ethanol from a tank with conductive walls. Upward convection of clean air, heated by the outer surface of the tank walls, entrains heavy air from the liquid surface and results in upward convection-driven evaporation. Similarity assumption is invalid in this case and temperature and vapor density fields cannot be obtained from BOS data.

References

[1] Gebhart B, Pera L (1971) The nature of vertical natural convection flows resulting from the combined buoyancy effects of thermal and mass diffusion. *International Journal of Heat and Mass Transfer*, vol. 14, pp 2025-2050. doi: 10.1016/0017-9310(71)90026-3

[2] Pera L, Gebhart B (1972) Natural convection flows adjacent to horizontal surfaces resulting from the combined buoyancy effects of thermal and mass diffusion. *International Journal of Heat and Mass Transfer*, vol. 15, pp 269-278. doi: 10.1016/0017-9310(72)90074-9

[3] El-Wakil M M, Myers G E, Schilling R J (1966) An interferometric study of mass transfer from a vertical plate at low Reynolds numbers. *Journal of Heat Transfer*, vol. 88, pp 399-406. doi: 10.1115/1.3691585

[4] Lee T S, Parikh P G, Acrivos A, Bershader D (1982) Natural convection in a vertical channel with opposing buoyancy forces. *International Journal of Heat and Mass Transfer*, vol. 25, pp 499-511. doi: 10.1016/0017-9310(82)90053-9

[5] Dehaeck S, Rednikov A, Colinet P (2014) Vapor-based interferometric measurement of local evaporation rate and interfacial temperature of evaporating droplets. *Langmuir*, vol. 30, pp 2002-2008. doi: 10.1021/la404999z

[6] Kelly-Zion P L, Pursell C J, Hasbamrer N, Cardozo B, Gaughan K, Nickels K (2013) Vapor distribution above an evaporating sessile drop. *International Journal of Heat and Mass Transfer*, vol. 65, pp 165-172. doi: 10.1016/j.ijheatmasstransfer.2013.06.003

[7] Souza Mendes P R (1991) The naphthalene sublimation technique. *Experimental Thermal and Fluid Science*, vol. 4, pp 510-523. doi: 10.1016/0894-1777(91)90031-L

[8] Goldstein R J, Cho H H (1995) A review of mass transfer measurements using naphthalene sublimation. *Experimental Thermal and Fluid Science*, vol. 10, pp 416-434. doi: 10.1016/0894-1777(94)00071-F

[9] Sparrow E M, Niethammer J E (1979) Natural convection in a ternary gas mixture – application to the naphthalene sublimation technique. *Journal of Heat Transfer*, vol. 101, pp 404-410. doi: 10.1115/1.3450988

[10] Meier G E A (2002) Computerized Background-Oriented Schlieren. *Experiments in Fluids*, vol. 33, pp 181-187. doi: 10.1007/s00348-002-0450-7

[11] Vinnichenko N, Plaksina Yu, Yakimchuk O, Soldatenkova K, Uvarov A (2017) Air flow temperature measurements using infrared thermography. *Quantitative InfraRed Thermography Journal*, vol. 14, pp 107-121. doi: 10.1080/17686733.2016.1258149

[12] Kotchourko N, Kuznetsov M, Kotchourko A, Grune J, Lelyakin A, Jordan T (2014) Concentration measurements in a round hydrogen jet using Background Oriented Schlieren (BOS) technique. *International Journal of Hydrogen Energy*, vol. 39, pp 6201-6209. doi: 10.1016/j.ijhydene.2013.10.152

[13] Vinnichenko N A, Pushtaev A V, Plaksina Yu Yu, Rudenko Yu K, Uvarov A V (2018) Horizontal convection driven by nonuniform radiative heating in liquids with different surface behavior. *International Journal of Heat and Mass Transfer*, vol. 126, pp 400-410. doi: 10.1016/j.ijheatmasstransfer.2018.06.036

[14] Vinnichenko N A, Uvarov A V, Plaksina Yu Yu (2014) Combined study of heat exchange near the liquid–gas interface by means of Background Oriented Schlieren and Infrared Thermal Imaging. *Experimental Thermal and Fluid Science*, vol. 59, pp 238-245. doi: 10.1016/j.expthermflusci.2013.11.023